Magnetization Reversal of the Domain Structure in the Anti-Perovskite Nitride Co_3FeN investigated by high-resolution x-ray microscopy

T. Hajiri,[1,*] S. Finizio,[2,†] M. Vafaee,[2] Y. Kuroki,[1] H. Ando,[1] H. Sakakibara,[1]
A. Kleibert,[3] L. Howald,[3] F. Kronast,[4] K. Ueda,[1] H. Asano,[1] and M. Kläui[2]

[1]*Department of Crystalline Materials Science, Nagoya University, Nagoya 464-8603, Japan*

[2]*Institut für Physik, Johannes Gutenberg Universität, Staudingerweg 7, Mainz, D-55128, Germany*

[3]*Swiss Light Source, Paul Scherrer Institut, Villigen, CH-5232, Switzerland*

[4]*Helmholtz-Zentrum Berlin für Materialien und Energie GmbH, Albert-Einstein-Straße 15, D-12489, Berlin, Germany*

(Dated: January 26, 2017)

Abstract

We performed X-ray magnetic circular dichroism photoemission electron microscopy to reveal the magnetic domain structure of anti-perovskite nitride Co_3FeN exhibiting a negative spin polarization. In square and disc patterns, we systematically and quantitatively determine the statistics of the stable states as a function of geometry. By direct imaging during the application of a magnetic field, we reveal the magnetic reversal process in a spatially resolved manner. We compare the hysteresis on the continuous area and the square patterns from the magnetic field-dependent XMCD ratio, which can be explained as resulting from the effect of the shape anisotropy, present in nanostructured thin films.

I. INTRODUCTION

3d transition metal ferromagnets have been widely studied for applications in spintronic devices such as magnetoresistive random-access memory [1], as the high spin polarization of their conduction electrons is of great interest for spintronic applications, such as e.g. the racetrack or the vortex random-access memories [2–4]. Amongst the several ferromagnetic 3d transition metal compounds, anti-perovskite nitrides exhibit unique magnetic properties, which could open new avenues for the fabrication of more efficient spintronic systems. For example, the typical compound Fe_4N is expected to exhibit a negative spin polarization with the spin polarization of the electrical conductivity expected to be -100%, while the spin polarization at the Fermi energy is calculated to be about -60 % [5]. Actually, the absolute value of the spin polarization of Fe_4N was reported to be $|59\%|$ at $T = 7.8$ K by point contact Andreev reflection spectroscopy [6]. Furthermore, the negative spin polarization was confirmed by an inverse tunneling magnetoresistance ratio of -76 % in Fe_4N/MgO/CoFeB magnetic tunnel junctions measured at room temperature [7]. Therefore, thanks to the possibility to generate a highly negative spin polarized current, Fe_4N and related compositions are of great interest for applications in more efficient spintronic systems in combination with positive spin polarization materials.

Due to these intriguing properties, related anti-perovskite nitrides such as $Co_xFe_{4-x}N$ have also been studied [8]. Among the $Co_xFe_{4-x}N$ series, Co_3FeN (CFN) is theoretically expected to exhibit a half-metallic behavior with a negative spin polarization [9], therefore making this particular Co-based nitride of great interest. Up to now, CFN thin films were fabricated by reactive magnetron sputtering on $(LaAlO_3)_{0.3}$–$(SrAl_{0.5}Ta_{0.5}O_3)_{0.7}(001)$ (LSAT) substrates [10] and by molecular beam epitaxy on $SrTiO_3(001)$ substrates [8], where a large negative anisotropic magnetoresistance was observed also at room temperature for both deposition methods. As negative AMR is considered to be related to half-metallicity [11, 12], the measurements reported in Refs. [8, 10] exhibit additional evidence that this material exhibits, as theoretically predicted, a half-metallic behavior. Furthermore, the possibility of current-induced magnetization switching of uncompensated antiferromagnetic spins was reported in anti-perovskite ferromagnet/antiferromagnet Co_3FeN/Mn_3GaN epitaxial bilayers [13], which provided an additional avenue for the use of electrical currents to control the magnetization configuration of nanostructured materials. However, if such interesting

material is to be employed for spintronic applications, it is important to clarify the magnetic domain structure of confined geometrical nanostructures, and the process of magnetization reversal induced by the application of an external magnetic field and current.

The magnetic domain structure of typical $3d$ transition metal has been under intense study (see, e.g., Refs. [14, 15]). Generally, the main contributions to the magnetic free energy of such a material are given by the exchange energy, magnetocrystalline anisotropy, shape anisotropy, stray field and the Zeeman energy [14, 15]. In particular, the competition between magnetocrystalline anisotropy and shape anisotropy can be employed to control the magnetization configuration in structured ferromagnetic elements [14]. Depending on the specific systems, one or more of these terms will be dominant: e.g. in Py nanostructures, shape anisotropy dominates while, e.g. in Co_2MnGa nanostructures, the magnetic configuration is the result of the interplay between shape and magnetocrystalline anisotropy [16]. However, almost all of the above mentioned studies have been performed with positive spin polarization materials, and no in-depth characterization of the magnetic domain structure of negative spin polarized materials has been, as of yet, carried out.

Moreover, shape (or intrinsic configurational [17]) anisotropy can affect the magnetization reversal process [18]. The effect of shape anisotropy has been mainly studied by measuring magnetic hysteresis loops as a function of pattern shape, size and thickness [19]. To explore the magnetic reversal process of geometrical nanostructures exhibiting a negative spin polarization, a direct observation of change of the domain structure during the magnetization reversal is thus needed.

In this work, we performed X-ray magnetic circular dichroism photoemission electron microscopy (XMCD-PEEM) measurements aimed at the determination of the magnetic domain structure of confined geometrical CFN nanostructures, which exhibits a negative spin polarization. We find that shape anisotropy is more dominant than magnetocrystalline anisotropy for smaller confined nanostructures of about 1 μm due to the increasing confinement. We observed the magnetic field-dependent XMCD ratio and magnetic domain structure corresponding to the nanostructure hysteresis loop, allowing us to analyze the effect of shape anisotropy on the magnetic reversal process.

II. EXPERIMENTAL DETAILS

High-quality epitaxial CFN(001) thin films (50 nm) with an Al capping layer (3 nm) were fabricated by reactive magnetron sputtering on LSAT(001) substrates as described elsewhere [10]. The magnetic properties of the continuous CFN films were characterized, before the patterning of the nanostructures that were analyzed with XMCD-PEEM imaging, with vibrating sample magnetometry and magneto-optic Kerr effect (MOKE) magnetometry measurements using a longitudinal MOKE setup with red (635 nm) low noise laser diode at room temperature before the XMCD-PEEM measurements. The CFN films were then patterned using focused ion beam lithography to define micrometer to sub-micrometer scale patterns. XMCD-PEEM measurements were performed at the SIM (X11MA) beamline at the Swiss Light Source [20] and at the UE49-PGMa beamline at the synchrotron radiation facility (BESSY) of the Helmholtz-Zentrum Berlin [21], both equipped with an Elmitec PEEM setup (type LEEM III). The energy of the circularly polarized x-rays was tuned to the Co L_3 edge (about 780 eV). No changes in the magnetic configuration of the material were observed upon tuning the x-ray energy to the Fe L_3 edge (ca. 707 eV), thus confirming that, as expected, both the Fe and Co moments are aligned parallel to each other. The patterned CFN films were demagnetized by an ac magnetic field just before the XMCD-PEEM measurements. All XMCD-PEEM measurements except the field-induced measurements were performed in a virgin state.

III. RESULTS AND DISCUSSIONS

The magnetic properties of the as-grown CFN films are shown in Fig. 1. An angular dependence of the ratio between the remnant and the saturation magnetization, M_r/M_s, of CFN is shown in Fig. 1(a), showing that the CFN films exhibit a clear 4-fold magnetocrystalline anisotropy with the easy axis oriented along the $\langle 110 \rangle$ crystalline directions and the hard axis along the $\langle 100 \rangle$ crystalline directions of the CFN film. The two hysteresis loops acquired along the easy and hard axes of the CFN films are shown in Fig. 1(b). To determine the magnitude of the two and four-fold anisotropy constants K_u and K_1 of the CFN thin film, we analyzed the data with the Stoner-Wohlfarth model [22]. As the Stoner–Wohlfarth model does not describe the formation of magnetic domains, we applied the model to fit the

reversible part of the measured hysteresis loop along the hard-axis of the CFN films, which yields the anisotropy parameter reliably as reported for other materials [16, 23, 24]. As shown in Fig. 1(c), it is possible to fit the reversible part of the hysteresis loop assuming a four-fold anisotropy constant K_1 of 34850 ± 250 J/m^3, without any uniaxial anisotropy contribution in line with the results shown in Fig. 1(a). The estimated value of K_1 is comparable with that of Fe_4N ($K_1 \sim 29000$ J/m^3) [25].

Next, we turn our attention on the spin structure in analysis of the nanostructured CFN elements. The XMCD-PEEM images in Fig. 2(a) show the magnetic configuration of CFN nanostructured squares with their edges aligned parallel to the easy axes [along the [110] and [1$\bar{1}$0] directions as shown in Fig. 1(a)]. In this configuration, the 4-fold magnetocrystalline anisotropy and shape anisotropy cooperate, resulting in the stabilization of flux-closure Landau patterns, with a few exceptions, as shown in Fig. 2(b). These distorted Landau states can be interpreted by considering an additional uniaxial anisotropy contribution [24], which can occur due to local variations in the quality of the thin films, or to the effect of step-edges caused by substrate miscuts [24]. The other possibility is that the distorted Landau patterns can also be metastable states, which is stabilized by the pinning of wall edge clusters at defects in the element edges [14]. All of them are unavoidable in experimental systems. When the square edges are oriented parallel to the hard axes [along the [100] and [010] directions as shown in Fig. 1(a)], magnetocrystalline and shape anisotropy are now competing with one another, stabilizing more complex magnetic states. As shown in Figs. 2(c) and 2(d), both simple Landau state and more complex magnetic states can be stabilized when the square edges are parallel to the hard axes. To determine the magnetic configuration of the nanostructured squares with their edges along the hard axes of the CFN, we acquired XMCD-PEEM images at different sample rotating. Figure 3 shows the XMCD-PEEM images acquired at an angle of 0° (top panels) and 45° (middle panels) with respect to the square edge, and the calculated two dimensional (2D) vector maps [26] (bottom panels). As shown in the magnetic 2D vector maps, all the stable non-Landau magnetic states are in magnetic configurations that resemble the magnetic S state. Both simple and more complex S states are stabilized, as shown in Fig. 3. The ratio of flux-closure Landau states with respect to S states are 85.7 % among the total 49 imaged squares of 3 μm, 84.8 % among the total 46 imaged squares of 2 μm, 92.9 % among the total 42 imaged squares of 1 μm and 97.7 % among the total 43 imaged squares of 0.5 μm. In the case of square edges aligned

parallel to the easy axes, no S states were observed. These results suggest that the smaller the structure the more shape anisotropy dominates; that is, flux-closure Landau pattern are the energetically favored magnetic configuration, and S states originate from the competition between magnetocrystalline anisotropy and shape anisotropy [23, 27].

A similar behavior to the nanostructured CFN squares was observed in the nanostructured CFN disc structures. Most of the nanostructured discs stabilize a flux-closure vortex state but the 0.5 μm disc is possibly a distorted flux closure state, as shown in Fig. 4(a). On the other hand, more complex magnetic structures were observed in the 3 μm and 2 μm discs. To investigate these more complex magnetic structures, we acquired angle-dependent XMCD-PEEM images to determine the magnetization 2D vector maps in a similar manner as for the nanostructured squares. Such magnetization 2D vector maps are shown in Fig. 4(b). Once again, more complex magnetic structures appear that exhibit a state resembling an S state with a vortex. The ratio of flux-closure vortex state in the disc patterns with respect to the complex states are 88.0 % among the total 25 imaged disks with a diameter of 3 μm, 96.0 % among the total 25 imaged disks with a diameter of 2 μm, 100.0 % among the total 16 imaged disks with a diameter of 1 μm and 100.0 % among the total 20 imaged disks with a diameter of 0.5 μm. Figure 4(c) shows the comparison of the schematic domain structure of this work with a typical uniaxial anisotropy [14]. The magnetic domain structure with uniaxial anisotropy shows a three domain state, and spins align parallel to the easy axis direction. Similarly, in this study, spins align parallel to the four-fold easy axis direction, suggesting a strong contribution of the four-fold magnetocrystalline anisotropy to the magnetic domain structure in disc elements. This feature appears much stronger than that of other four-fold anisotropy material [16, 23, 27], possibly due to the large magnetocrystalline anisotropy constant K_1. Therefore, these complex magnetic domain structures are also considered to result from the competition between magnetocrystalline and shape anisotropy [23, 27].

After clarifying the magnetic domain structure of the confined geometries, we finally turn our attention to the influence of external magnetic fields on the magnetic domain structure of the 1 μm square pattern CFN elements to clarify the effect of shape anisotropy for the magnetization reversal process. The magnetic field-dependent domain structure of a typical 1 μm square pattern with its edges oriented along the CFN hard axes is shown in Fig. 5. Because this material exhibits no strong pinning and a clearly visible displacement of vortex core is important to understand the hysteresis loop and the eventual presence

of pinning points in the nanostructured elements, we chose a Landau state as the virgin state. Upon applying a magnetic field of about 24 mT parallel along the hard axis, we observe a non-saturated domain structure, as shown in upper-right panel of Fig. 5(a), which can be interpreted as a deformed Landau state (i.e. the vortex core is displaced by the application of a magnetic field). We should note that 24 (-21) mT was the maximum field we could apply in the PEEM while imaging. Upon a further reduction of the magnetic field down to about -21 mT, the domain structures changes at magnetic field magnitudes between 0 and -4.5 mT and between -12 and -15 mT. At $H = -21$ mT, the domain structure does not saturate. Upon the application of a saturating field of about -35.5 mT, followed by its relaxation down to about -21 mT, we were able to observe a saturated quasi single-domain state. The application of a positive or negative magnetic field leads to some substantial changes in the magnetic configuration. In particular, such changes occur at applied fields between 0 and 6 mT and between 12 and 15 mT. The average XMCD ratio of the square pattern, calculated by averaging the recorded intensity in the single XMCD images, is also shown in Fig. 5(b). To compare with the nanostructured elements, the XMCD ratio of a continuous CFN area was also recorded. Here, a clear difference with respect to the square elements was observed. In particular, the XMCD hysteresis loop shape is different between square patterns and the continuous film area. [28] When compared with the MOKE measurements of the continuous CFN films, the XMCD-PEEM measurements of the continuous area show a good agreement with the MOKE hysteresis, although those of the square patterns are different from the recorded MOKE hysteresis loops. Up to now, there is no report about shape anisotropy of CFN, but these different shape of the hysteresis loop between structured elements and continuous films have been reported for many $3d$ transition metal thin films, where the influence of shape anisotropy was used to explain the results [15, 18, 19, 29, 30]. Therefore, we conclude that the obtained domain structures as well as XMCD hysteresis loops results from the interplay between the Zeeman energy of the applied field and the shape anisotropy due to the geometrical confinement.

IV. SUMMARY

We performed XMCD-PEEM measurements to determine the magnetic configuration of nanostructured elements of the anti-perovskite nitride CFN, which exhibits a negative spin

polarization. We observed Landau and vortex states in square and disc structures and more complex magnetic domain structures were observed for larger structures in particular if magnetocrystalline anisotropy and shape anisotropy compete against each other. We analyzed the dependence of the magnetic configuration of the nanostructured CFN elements upon the application of an external field, observing distinct features in the magnetic hysteresis loops that are only present in nanostructured thin films, suggesting an influence of shape anisotropy. These results provide a new insight into the effects of shape anisotropy and the Zeeman energy on the magnetization reversal processes of nanostructures for spintronic application field using a negative spin polarization materials. And for CFN, our results show that, by tuning the geometry, stable and reproducible spin structures with clear switching characteristics can be obtained, making this material apt for possible devices.

ACKNOWLEDGMENTS

Part of this work was performed at the Swiss Light Source and at the BESSY II light source. This work was supported by JSPS Program for Advancing Strategic International Networks to Accelerate the Circulation of Talented Researchers, the EU 7$^{\text{th}}$ Framework Programme IFOX (NMP3-LA-2010 246102), CALIPSO (FP7/2007-2013 312284), the European Research Council through the Starting Independent Researcher Grant MASPIC (ERC-2007-StG 208162), SNF, and DFG as well as the Graduate School of Excellence Materials Science in Mainz (GSC 266).

---

* Electronic mail: t.hajiri@numse.nagoya-u.ac.jp

† Present address: Swiss Light Source, Paul Scherrer Institut, Villigen PSI, CH-5232, Switzerland

[1] J. Åkerman, Science **308**, 508 (2005).

[2] S. A. Wolf, D. D. Awschalom, R. A. Buhrman, J. M. Daughton, S. von Molnár, M. L. Roukes, A. Y. Chtchelkanova, and D. M. Treger, Science **294**, 1488 (2001).

[3] S. S. P. Parkin, M. Hayashi, and L. Thomas, Science **320**, 190 (2008).

[4] S. Bohlens, B. Krüger, A. Drews, M. Bolte, G. Meier, and D. Pfannkuche, Appl. Phys. Lett. **93**, 142508 (2008).

[5] S. Kokado, N. Fujima, K. Harigaya, H. Shimizu, and A. Sakuma Phys. Rev. B **73**, 172410 (2006).

[6] A. Narahara, K. Ito, T. Suemasu, Y. K. Takahashi, A. Ranajikanth, and K. Hono, Appl. Phys. Lett. **94**, 202502 (2009).

[7] K. Sunaga, M. Tsunoda, K. Komagaki, Y. Uehara, and M. Takahashi, J. Appl. Phys. **102**, 013917 (2007).

[8] K. Ito, K. Kabara, T. Sanai, K. Toko, Y. Imai, M. Tsunoda and T. Suemasu, J. Appl. Phys. **116**, 053912 (2014).

[9] Y. Takahashi, Y. Imai, and T. Kumagai, J. Magn. Magn. Mater. **323**, 2941 (2011).

[10] H. Sakakibara, H. Ando, T. Miyawaki, K. Ueda, and H. Asano, IEEE Trans. Magn. **50**, 2600404 (2014).

[11] S. Kokado, M. Tsunoda, K. Harigaya, and A. Sakuma, J. Phys. Soc. Jpn. **81**, 024705 (2012).

[12] Y. Sakuraba, S. Kokado, Y. Hirayama, T. Furubayashi, H. Sukegawa, S. Li, Y. K. Takahashi, and K. Hono, Appl. Phys. Lett. **104**, 172407 (2014).

[13] H. Sakakibara, H. Ando, Y. Kuroki, S. Kawai, K. Ueda, and H. Asano, J. Appl. Phys. **117**, 17D725 (2015).

[14] A. Hubert and R. Schäfer, Magnetic Domains: The Analysis of Magnetic Microstructures (Springer-Verlag, Berlin Heidelberg, 1998).

[15] M. Kläui and C. A. F. Vaz, Handbook of Magnetism and Advanced Magnetic Materials, edited by H. Kronmüller and S. S. P. Parkin (Wiley & Sons, New York, 2007), Vol. 2.

[16] S. Finizio, A. Kronenberg, M. Vafaee, M. Foerster, K. Litzius, A. de Lucia, T. O. Menteş, L. Aballe, B. Krüger, M. Jourdan, and M. Kläui, New J. Phys. **17**, 083030 (2015).

[17] B. K. Mahato, S. Choudhury, R. Mandal, S. Barman, Y. Otani, and A. Barman, J. Appl. Phys. **117**, 213909 (2015).

[18] R. P. Cowburn, A. O. Adeyeye, and M. E. Welland, Phys. Rev. Lett. **81**, 5414 (1998).

[19] R. P. Cowburn, D. K. Koltsov, A. O. Adeyeye, and M. E. Welland, Europhys. Lett. **48**, 221 (1999).

[20] L. Le Guyader, A. Kleibert, A. F. Rodríguez, S. EI Moussaoui, A. Balan, M. Buzzi, J. Raabe, and F. Nolting, J. Electron Spectrosc. Relat. Phenom. **185**, 371 (2012).

[21] F. Kronast, J. Schlichting, F. Radu, S. K. Mishra, T. Noll, and H. A. Dürr, Surf. Interface Anal. **42**, 1532 (2010).

[22] E. C. Stoner and E. P. Wohlfarth, Philos. Trans. R. Soc. London A **240**, 599 (1948).

[23] T. Miyawaki, M. Foerster, S. Finizio, C. A. F. Vaz, M.-A. Mawass, K. Inagaki, N. Fukatani, L. Le Guyader, F. Nolting, K. Ueda, H. Asano, and M. Kläui, J. Appl. Phys. **114**, 073905 (2013).

[24] M. S. Gabor, T. Petrisor Jr., C. Tiusan, M. Hehn, and T. Petrisor, Phys. Rev. B **84**, 134413 (2011).

[25] J. L. Costa-Krämer, D. M. Borsa, J. M. García-Martín, M. S. Martín-González, D. O. Boerma, and F. Briones, Phys. Rev. B **69**, 144402 (2004).

[26] See supplementary material regarding the calcurated 2D vector map.

[27] C. A. F. Vaz, J. Rhensius, J. Heidler, P. Wohlhüter, A. Bisig, H. S. Körner, T. O. Mentes, A. Locatelli, L. Le Guyader, F. Nolting, T. Graf, C. Felser, L. J. Heyderman, and M. Kläui, Appl. Phys. Lett. **99**, 182510 (2011).

[28] Smaller M_s of the nanostructured elements than the continuous area might indicate that patterning the film affects the stoichiometry and therefore, affect the saturated magnetization.

[29] J. Yu, U. Rüdiger, A. D. Kent, L. Thomas, and S. S. P. Parkin, Phys. Rev. B **60**, 7352 (1999).

[30] M. Hehn, K. Ounadjela, J. P. Bucher, F. Rousseaux, D. Decanini, B. Bartenlian, and C. Chappert, Science **272**, 1782 (1996).

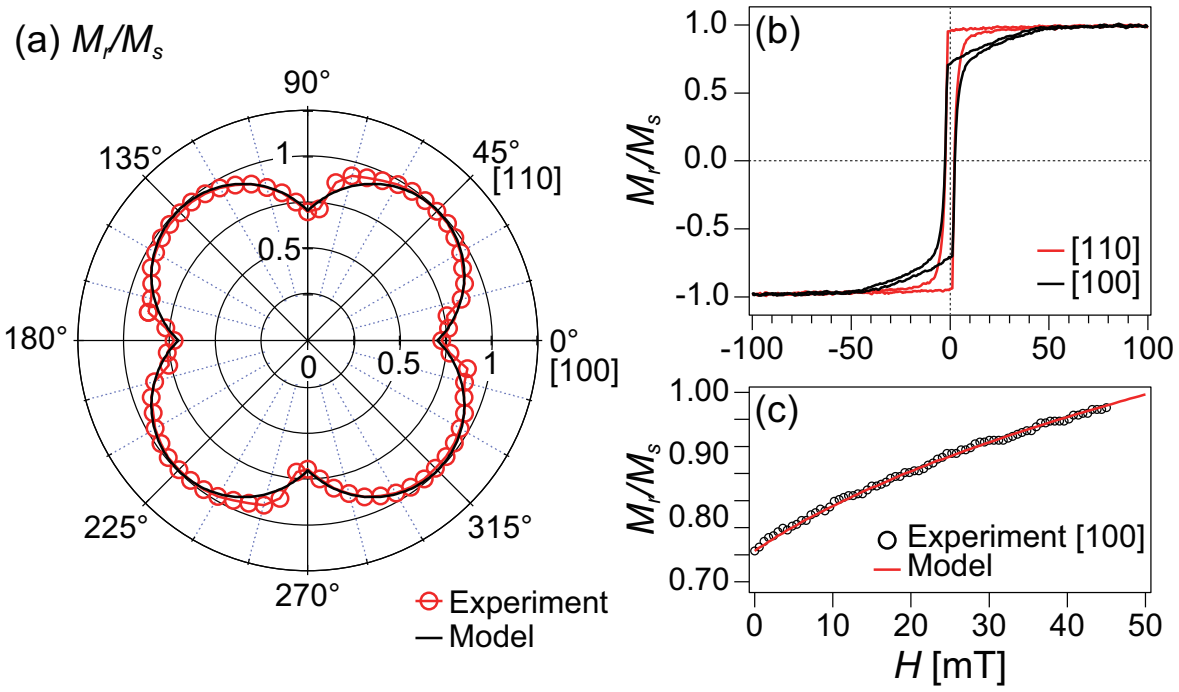

FIG. 1. (a) Angular dependence of M_r/M_s. Solid line is estimated from the Stoner–Wohlfarth model using $K_1 = 34850$ J/m^3. (b) Magnetic hysteresis loops along easy axis [110] and hard axis [100]. (c) Comparison of magnetic hysteresis loop sections along the hard axis [100] with simulations using $K_1 = 34850$ J/m^3.

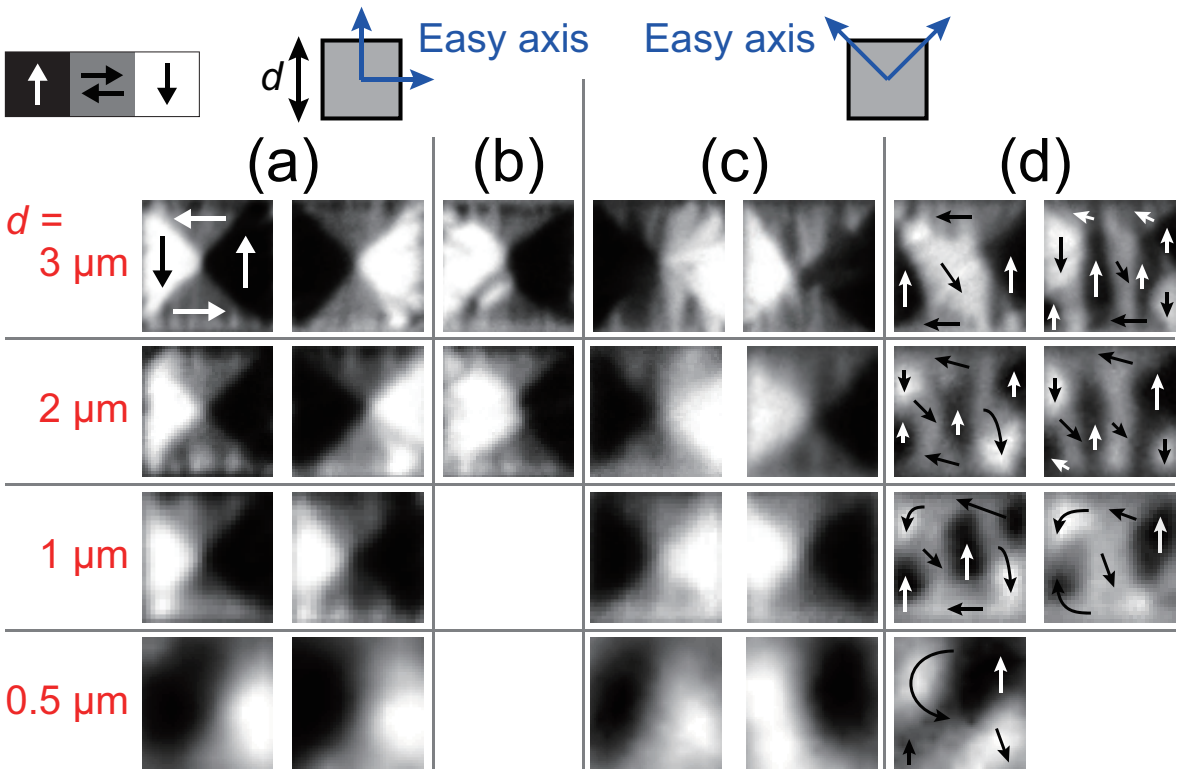

FIG. 2. XMCD-PEEM images of various sizes square patterns in a virgin state. (a),(b) Square edges parallel to the easy axes. Most magnetic domain structures of this configuration show simple Landau states (a), but some show distorted Landau states (b). (c),(d) Square edges parallel to the hard axis. Most magnetic domain structure also show simple Landau states (c), but a significant number show complex S states (d).

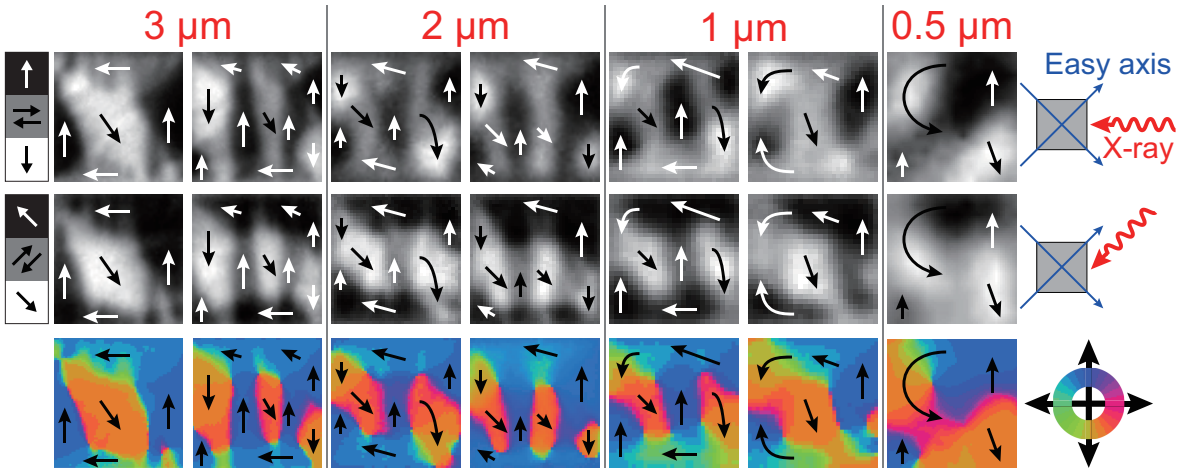

FIG. 3. XMCD-PEEM images in a virgin state with contrast directions along 0° (top) (along the edges) and 45° (middle) (along the diagonal). Resulting 2D vector maps are shown in bottom panels. The samples are aligned so that the square edge is parallel to the hard axis.

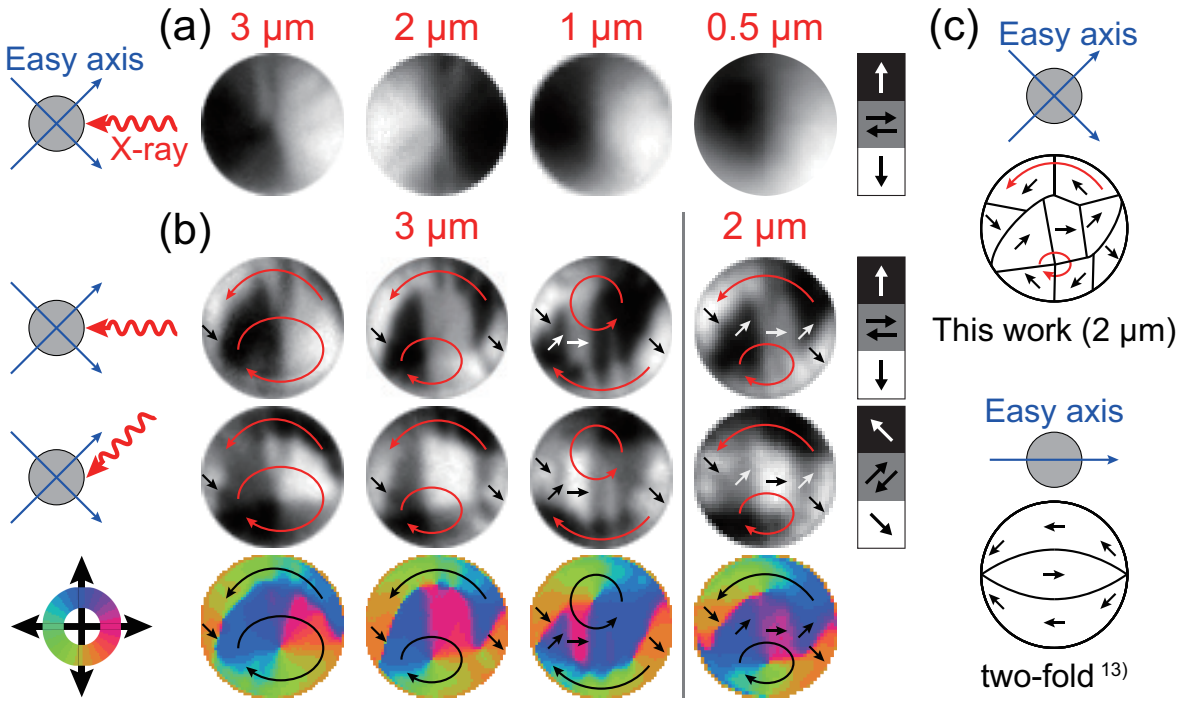

FIG. 4. Series of XMCD-PEEM images in a virgin state. (a) The vortex state of several disc sizes. (b) Complex magnetic domain structures with contrast directions along 45° (top) and 0° (middle) with respect to the easy axis in 3 μm and 2 μm discs. Resulting 2D vector maps are shown in botom panels. (c) Comparing schematic domain structure between this work and typical uniaxial anisotropy [14].

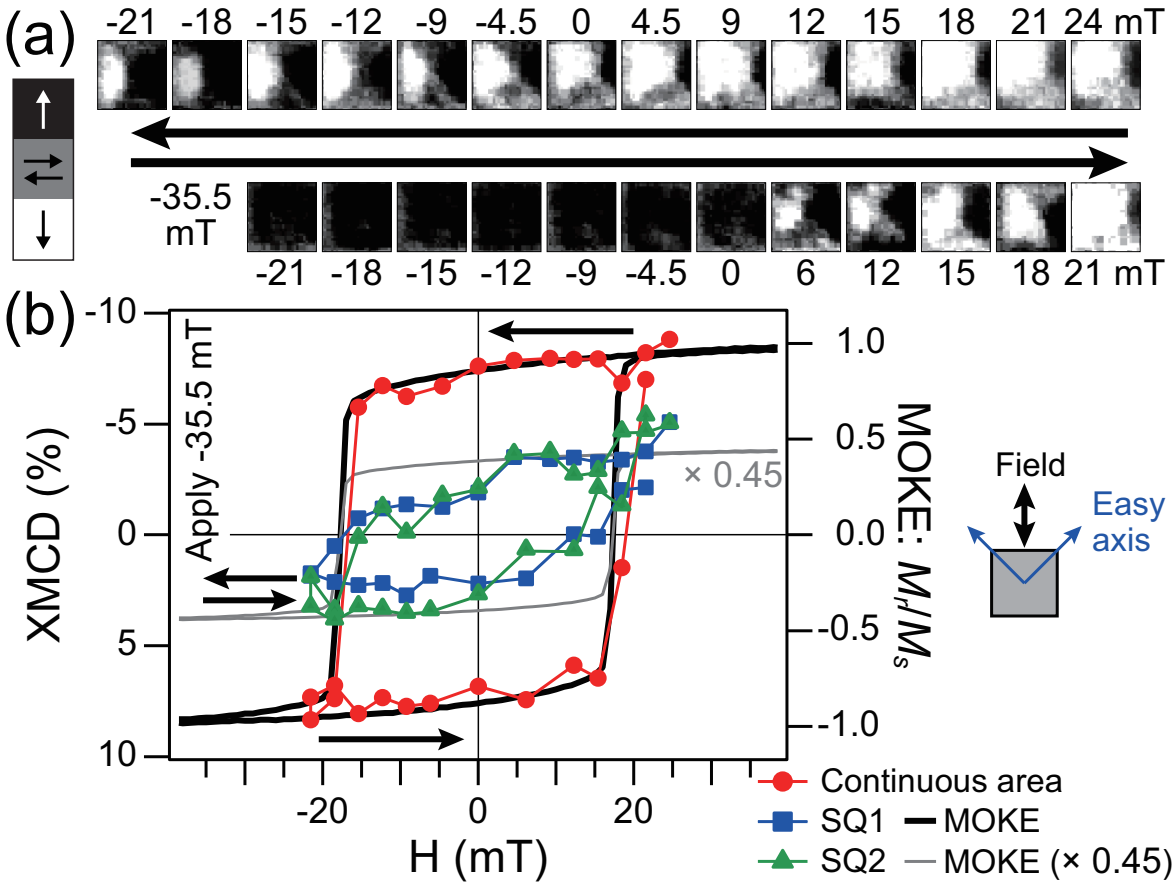

FIG. 5. Magnetic field dependent XMCD ratio and magnetic domain structure of 1μm square patterns. The magnetic field was applied parallel to the hard axis. The square edge is aligned parallel to the hard axis. SQ1 and SQ2 were two different squares that stabilized in the flux-closure Landau states. The magnetic domain structures are corresponding to structure SQ2.